Effect of Transition-Metal Cations on the Adsorption of H_2S in Modified Pillared Clays

Danh Nguyen-Thanh[†] and Teresa J. Bandosz*[,‡]

Department of Chemistry, The City College of the City University of New York, and The Graduate School of the City University of New York, New York 10031

Received: October 31, 2002; In Final Form: March 26, 2003

Sodium montmorillonite was intercalated with the Keggin ion (hydroxyaluminum polycation) and calcined at 400 °C. Then, doping with Fe^{3+}, Cu^{2+}, or Zn^{2+} was carried out. On the obtained samples, H_2S breakthrough capacity tests were carried out under wet conditions. Doping with metals significantly improved the capacity of adsorbents, despite a noticeable decrease in microporosity. The sample doped with copper showed the best performance as a hydrogen sulfide adsorbent. The reason for this is likely the affinity of the metal to bind hydrogen sulfide, the degree of metal dispersion, and the accessibility of small pores.

Introduction

From their first syntheses during the late 1970s,[1−3] PILCs (pillared interlayered clays) have attracted a lot of attention and have been the subject of numerous studies. They are generated through the exchange of the small charge-compensating cations (usually alkali) of the clays, situated between the negatively charged clay layers, with metal polyoxycations.[4,5] Calcination at 400 °C or higher temperatures leads to the dehydration and dehydroxylation of hydroxycations and their conversion to metal oxide pillars separating the clay layers.[4,6,7] Hence, for example, pillaring a clay with Al implies first the intercalation of the Keggin ion $[AlO_4Al_{12}(OH)_{24}(H_2O)_{12}]^{7+}$ [8,9] and then the formation of Al_2O_3 pillars as a result of heat treatment.[9−12]

Pillaring of clay with metal oxides results in the appearance of new and interesting properties. First, the presence of these large pillars instead of alkali cations in the clay interlayer space causes the development of micropores (pores with a width smaller than 20 Å).[6,13,14−23] Another valuable feature of PILCs is their acidity, whether it is of the Brønsted or of the Lewis kind. Even though clays originally have Brønsted acidic character,[8] introducing metal oxide pillars, especially aluminum, brings Lewis acid sites.[12] These properties explain why PILCs have been so extensively studied. They are potentially good materials for many industrial applications, mostly in catalysis[4,6,24] and gas adsorption.[7] But so far, most studies of PILC applications have been on their use as either catalysts or as catalyst supports. Meanwhile, studies using PILCs as gas adsorbents have been rather scarce.[25] Research on PILCs is currently going in new directions, one of them being the doping of PILCs with metallic cations.[12,26] This is done to introduce new acidic or oxido-reductive properties into the clay.

In this study, we synthesize transition-metal-doped Al PILCs and test them as adsorbents of hydrogen sulfide. Earlier studies showed that various adsorbents (carbonaceous and mineral) modified with metal cations have improved capacities for H_2S adsorption.[27−29] The metal cations used here for doping are Fe^{3+}, Zn^{2+}, and Cu^{2+}. They were chosen by taking into account either oxidation−reduction properties (iron) or the affinity of metals to form stable sulfides.

Experimental Section

Materials. Sodium Montmorillonite (Na−M). The same original (unmodified) clay was used for the preparation of all of the samples. It is a Na-rich montmorillonite from Crook County, Wyoming purchased from The Source Clay Minerals Repository from the University of Missouri in Columbia. In all experiments, it was used as received without any purification.

Al-Pillared Montmorillonite (Al−M). For Al pillaring, a 50 wt % solution of chlorhydrol from Reheis Inc. was used. It is a solution of aluminum chlorohydrate, which has a molecular formula of $Al_2Cl(OH)_5\cdot(2.5H_2O)$. The chlorhydrol was diluted with distilled water to give a 0.2 M solution with respect to aluminum content. The montmorillonite clay sample (20 g) was dispersed to water and aged for 24 h, and then the intercalating solution was added dropwise, giving a final Al/clay ratio of 20 mmol/g. The obtained suspension was stirred for 24 h at room temperature. Excess pillaring agent was washed out with distilled water until its conductivity reached 30 μS. After drying, the intercalated montmorillonite was obtained. The samples were calcined at 400 °C for 4 h. This process led to the formation of pillared montmorillonite, which is referred to as Al−M.[1,2,13,26,30,31]

Me-Doped Al-Pillared Montmorillonite (MeAl−M) with Me = Fe^{3+}, Zn^{2+}, Cu^{2+}. A 0.2 M NaCl solution (1 L) was prepared. Al−M (10 g) was dispersed into that solution with a Na/clay ratio of 20 mmol/g. The suspension was heated to 60 °C and stirred until all of the clay was well-dispersed. At that point, the pH of the solution was around 4.6. A dilute solution of 0.05 M NaOH was added dropwise to raise the pH of the suspension to 9. Once that pH was reached, small amounts of NaOH were added to maintain the pH at 9. After 24 h of stirring under these conditions, the suspension was washed by dialysis until the conductivity of the water was below 5 μS. Then the clay suspension was filtered and dried. A 20-g sample of treated Al−M was dispersed in 1 L of water, and 0.2 M solutions of either Fe^{3+}, Zn^{2+}, or Cu^{2+} were added dropwise until the Me/clay ratios were equal to 20 mmol/g. After the addition of the Me (iron, zinc, or copper) solution, the suspensions were stirred for 24 h. Then the clays were washed out using a dialysis membrane, filtered, dried, and calcined at 400 °C for 4 h. After

* To whom correspondence should be addressed. E-mail: tbandosz@ccny.cuny.edu. Tel: (212) 650-6017. Fax: (212) 650-6107.
[†] Department of Chemistry.
[‡] The Graduate School of the City University of New York.

10.1021/jp0223509 CCC: $25.00
Published on Web 05/23/2003

this process, the samples are referred to as AlFe−M, AlZn−M, and AlCu−M.

Methods. X-ray Diffraction (XRD). XRD (40 kV, 30 mA) was performed on a Rigaku X-ray diffractometer that uses Cu Kα (1.54184 Å) as a source of radiation. The analyzed clay samples were spread as thin layers on a glass slide. The diffraction patterns were obtained by varying the 2θ (θ being the Bragg angle) from 4 to 8° in increments of 0.008°.

N_2 Adsorption. N_2 adsorption measurements were performed at −193 °C on an ASAP 2010 (Micrometrics). In each case, about 0.2 g of sample was used. Prior to the measurement, all samples were degassed at 120 °C and until constant low pressure was reached (0.004 μm of Hg). For a precise determination of the microporosity, adsorption isotherms were measured at a very low relative pressure (P/P_o) of around 10^{-6}. Successive doses of N_2 were then added until the relative pressure reached 0.1. Then the preprogrammed pressure table was followed. The surface area, S_{N_2}, was calculated following the BET approach.[32] The total pore volume, V_t, was determined by nitrogen uptake at $P/P_o \approx 0.99$. The micropore volume, V_{mic}, and pore size distributions (PSDs) were obtained using the Kelvin equation with the Halsey thickness curve.[33−34]

Elemental Analysis. The Fe, Zn, and Cu contents of the different samples were determined using the ICP method of Huffman Laboratories (Golden, CO).

Thermal Analysis. Thermal analyses were carried out on an SDT 2960 from TA Instruments. The sample (about 20−30 mg) to be analyzed was heated from room temperature (∼30 °C) to 1000 °C at a rate of 10 °C/min with a flow of nitrogen at 100 mL/min. TG (thermal gravimetry) and DTG (derivative thermal gravimetry) curves were then recorded.

H_2S Breakthrough Capacity. Dynamic tests were carried out at room temperature to evaluate the capacity of the sorbents for H_2S removal under wet conditions. Adsorbent samples (2−3 mm granule size) were packed into a column (length 60 mm, internal diameter 9 mm, bed volume 6 cm^3) and prehumidified with moist air (relative humidity 80% at 25 °C) for 1.5 h. The amount of adsorbed water was estimated from the increase in the sample weight. Moist air containing 0.3% (3000 ppm) H_2S was then passed through the column of adsorbent at 0.5 L/min. The breakthrough of H_2S was detected using an Interscan LD-17 electrochemical sensor. The test was stopped at the breakthrough concentration of 1000 ppm. The adsorption capacities of each sorbent in terms of milligrams of H_2S per gram of adsorbent were calculated by integrating the area above the breakthrough curves and from the H_2S concentration in the inlet gas, the flow rate, the breakthrough time, and the mass of sorbent. For each sample, the H_2S test was repeated at least twice. The determined capacities agreed to within 5%.

To determine if sulfur dioxide was generated during H_2S adsorption/oxidation on modified clays, the SO_2 concentration in the effluent gas was also monitored with a MicroMax electrochemical sensor.

pH. The suspensions of clays were prepared by dispersing 0.4 g of the sample into 20 mL of water. They were stirred for 24 h and then filtered, and the pH of the filtrate was measured.

Results and Discussion

The X-ray diffraction patterns for our samples are presented in Figure 1. The Na−M sample shows a diffraction peak at $2\theta = 6.88°$, which, according to Bragg's law, corresponds to a basal spacing of 12.8 Å. Taking into account the thickness of a montmorillonite clay layer equal to 9.6 Å,[7,12] an interlayer spacing for this sample is equal to 3.2 Å. For Al−M with a diffraction peak at $2\theta = 5.08°$, the interlayer spacing is 7.8 Å.[31] This is in agreement with the expected values described in the literature.[4] After doping the clay with zinc and copper, the diffraction peaks are broader, but their maxima are at the same positions as that for the aluminum pillared material. It is interesting that AlFe−M lost its crystallinity as a result of the incorporation of iron and the delamination of the mineral structure.[35,36]

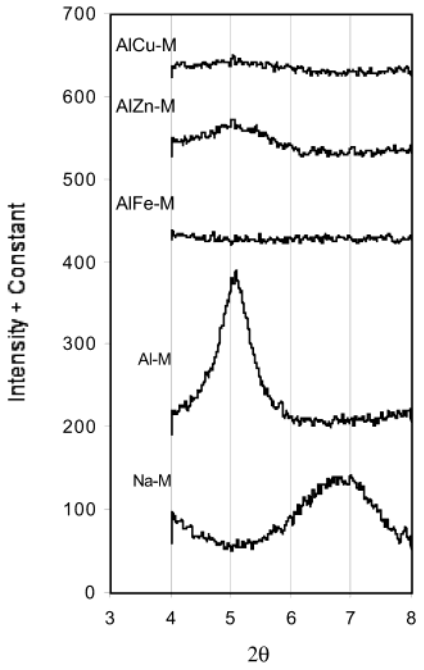

Figure 1. X-ray diffraction results.

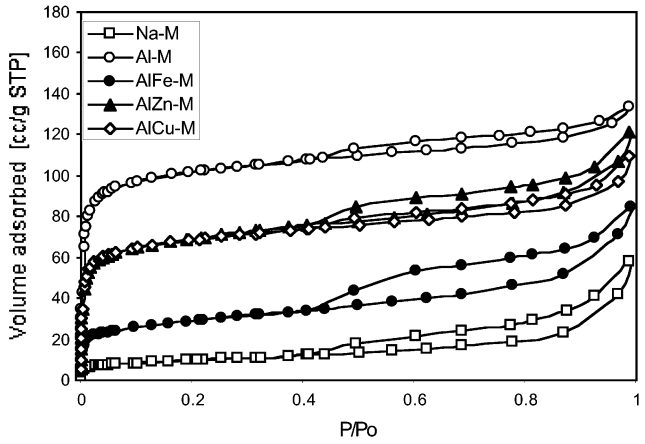

Figure 2. N_2 adsorption isotherms at −196 °C.

Although the N_2 adsorption isotherms of all of the clay samples are similar in shape (Figure 2), the amounts that were adsorbed significantly differ. After intercalation, nitrogen uptake significantly increased because of the formation of micropores as a result of the opening of the interlayer space for the nitrogen molecule. The steep rise at the beginning of the isotherms indicates the presence of microporosity. Doping with metals decreases the amount adsorbed and changes the width of the hysteresis loop, which indicates changes in the micro- and mesoporosity of the materials studied.[7,18] In the case of doping with iron, these changes are the most extended, suggesting the blocking of small pores along with the aggregation of mineral particles (changes in mesoporosity).[36] Both zinc and copper have similar effects on micropores; however, they affect larger pores differently. The hysteresis loop in the case of zinc is broader

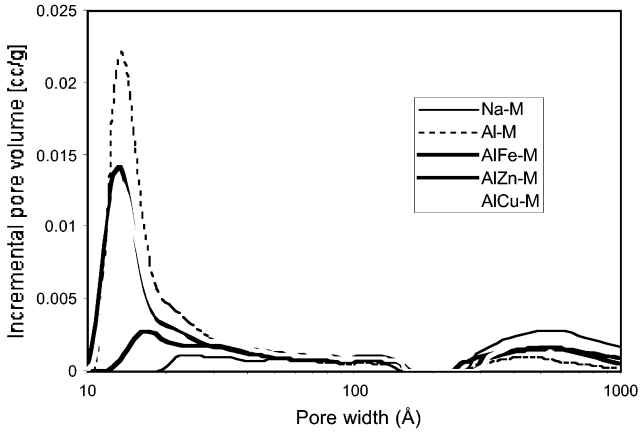

Figure 3. Pore size distributions.

TABLE 1: Structural Parameters Calculated from Nitrogen Adsorption Isotherms[a]

sample	S_{BET} [m^2/g]	V_{mic} [cm^3/g]	V_t [cm^3/g]
Na−M	34	0.001	0.090
Al−M	324	0.129	0.207
AlFe−M	97	0.017	0.131
Al−Fe−M/E	98	0.017	0.133
AlZn−M	228	0.091	0.161
AlZn−M/E	197	0.078	0.147
AlCu−M	220	0.082	0.169
AlCu−M/E	155	0.064	0.126

[a] E refers to the exhausted samples after H_2S adsorption.

than that for copper-doped material. The hysteresis loops are of type B for slit-shaped capillaries with parallel walls.[37] Such porosity is expected between the small particles of clays.[35,36]

Figure 3 collects pore-size distributions (PSDs). In the calculation of PSDs, the classical method (Kelvin equation with Halsey thickness curve) was used,[33,34] assuming that the pores have a cylindrical shape. So far, many approaches leading to the PSDs for PILC have been discussed in the literature, and none of them gives unambiguous results.[38−42] Because all of the materials have the same origin, in our view, the changes in pore structure can be compared if the same approach is used, even though it is not necessarily perfect. Figure 3 shows that all of the studied samples, besides the initial material and that modified with iron, have an intense peak at about 11 Å. The intensity of this peak corresponds to the volume of the pores. On the basis of XRD, the main pore size should be about 8 Å, and the shift is caused by the imperfection of the model that was used.[40,41] From the analyses of the obtained plots, it is clearly seen that after pillaring the volume of micropores significantly increased and doping with zinc or copper decreased it only slightly. This suggests that zinc and copper, as expected, are dopped on the mineral layers rather than on the surface of pillars. The PSD looks different for the sample modified with iron. For this material, the significant volume of the micropores is unavailable. As indicated above, it is likely due to the adsorption of metals on the external surface, delamination, and the aggregation of mineral particles.[36,43] Moreover, as indicated in the literature,[26] iron destroys the structural integrity of aluminum pillars.

Structural parameters calculated from the isotherms are collected in Table 1. After pillaring, the surface area increased 10-fold. Doping with zinc and copper has similar effects on the surface accessibility: the surface area decreases about 25% compared to that of the sample pillared with aluminum species. In the case of doping with iron, a 70% decrease in the surface area occurred. Similar changes are observed for the volume of micropores; in fact, they are expected because micropores mainly contribute to the surface of materials.[40] When the total pore volume is analyzed, the changes observed for the sample after doping with Fe^{3+} are not as drastic as changes in the surface area. This is the result of changes in the total pore structure of materials and the formation of new mesopores. This effect was observed previously for the samples modified with iron.[35,36,45]

Besides difference in the nature of surface interactions, changes in the pore volume can originate from differences in the amount of metal deposited on the surface. Elemental analysis showed that after modifications the content of metal was of 9.82, 4.03, and 7.72% for the iron-, zinc-, and copper-modified samples, respectively. Although the content of iron, which is twice that of zinc, can cause changes in the structure of the clay with pore blocking for AlFe−M, this is not the case when copper and iron are compared. This indicates that Cu^{2+} cations, besides being present in a highly dispersed state in micropores (small decreases in volume and pore size), are also present in significant quantities in mesopores and macropores. In the case of AlFe−M, the micropores practically do not exist. These differences can be caused by the propensity of iron to incorporate into aluminum pillars as a result of acid−base interactions.[26] This process leads to a decrease in the thermal stability of pillars and the collapse of the sorbent structure during calcination at 400 °C. It is likely that for AlZn−M, where the content of metals is twice smaller than for the copper-modified counterpart, Zn^{2+} cations are located mainly in the micropores.

The H_2S adsorption experiments carried out on Al−M showed negligible capacity; the sample was exhausted after 1.6 min, resulting in a breakthrough capacity of 0.6 mg of H_2S per g of sample. This happened even though the pore volume of the Al−M sample is quite significant compared to that of other adsorbents.[46] It has to be mentioned here that the physical adsorption of hydrogen sulfide under our experimental conditions is expected to be small because of the small size of the molecule and the high temperature of this process. The only factor that can enhance the capacity is chemisorption of hydrogen sulfide or its catalytic oxidation. In both of these cases, the pore volume is an important factor because the products of surface reactions, either salts or sulfur, have to be stored within the pore system of the adsorbents. The small capacity of Al−M obviously indicates the lack of any chemical or catalytic effect of the surface.

On the contrary, running the H_2S breakthrough experiment on the three doped samples, AlFe−M, AlZn−M, and AlCu−M, showed that doping with Me considerably improves the capacity of Al−M for H_2S adsorption. The breakthrough curves of the doped samples are shown in Figure 4. An analysis of the curve shapes suggests differences in the mechanisms of the removal of hydrogen sulfide on metal-modified pillared clays. For AlCu−M, the concentration rises linearly with a constant slope, suggesting a constant rate of the adsorption/reaction. However, the slope changes for the samples modified with zinc or iron. For these samples, after steep rises at the beginning, the slopes decrease. This indicates that after the initial step of adsorption the nature of the surface process changes, which is favorable for further retaining hydrogen sulfide.

Table 2 collects the breakthrough capacities for the materials studied. For AlCu−M, the capacity is almost 3 times higher than that for iron-modified counterparts. The capacity of AlZn−M is only slightly greater than that for AlFe−M. All of these differences follow neither the changes in the content of

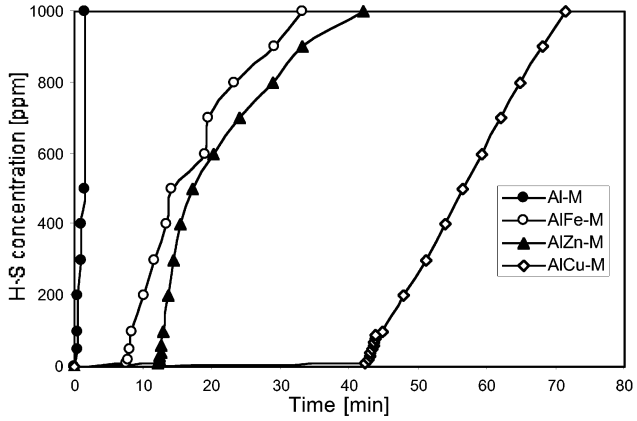

Figure 4. H_2S breakthrough curves.

TABLE 2: H_2S Breakthrough Capacity Results and pH of Surface

sample	weight [g]	bth time [min]	bth cap. [mg/g]	pH_{init}	pH_E
Al−M	5.29	1.60	0.60	7.18	
AlFe−M	3.28	33.23	17.64	5.59	5.59
AlZn−M	3.47	42.07	20.94	6.09	6.06
AlCu−M	2.83	71.27	48.77	5.35	5.05

metal nor the changes in the pore volumes. However, although the small adsorption on iron- and zinc-containing samples can be linked to the small pore volume or small metal content, respectively, the high adsorption on Cu-modified samples does not exactly follow the effect of metal loading. However, the comparison of the results obtained for the Zn- and Cu-modified samples does not stress the importance of the pore volume. The reason for the differences in the observed performance of the materials studied as H_2S adsorbents is in the combination of surface chemistry and porosity.

The analysis of the changes in the pore structure of the samples after adsorption may shed some light on the understanding of the H_2S removal mechanism of those materials.[47] The structural parameters are collected in Table 1. Comparison with the data obtained for exhausted samples to those for the samples not exposed to hydrogen sulfide adsorption clearly shows that in the case of zinc- and copper-modified samples the products of the adsorption/reaction are deposited on the surface, resulting in a decrease in the surface area and volume of pores. This decrease is the most pronounced for the sample modified with copper where the adsorption of hydrogen sulfide was the greatest.

Because the structural parameters for the iron-modified sample were unchanged after H_2S adsorption, in Figure 5 we collect the PSDs obtained for the samples modified with zinc and copper. For both samples, it is clearly seen that pores smaller than 200 Å are affected and that their volume is decreased. Although in the case of AlZn−M after H_2S adsorption the changes occurred mainly in the volume of mesopores, for AlCu−M/E the volume of the micropores is much more affected than that of mesopores. Although in the case of AlFe−M the amount of hydrogen sulfide adsorbed was similar to that on the zinc-modified sample, changes in the pore volume did not occur. It is likely that in the case of this sample Fe^{3+} was reduced to Fe^{2+}, thus oxidizing hydrogen sulfide to weakly adsorbed SO_2, which was desorbed from the surface immediately or during outgassing when high vacuum was applied.

Differences in the products of surface reactions are also seen in the values of the surface pH. Slightly basic Na−M (pH 7.18)

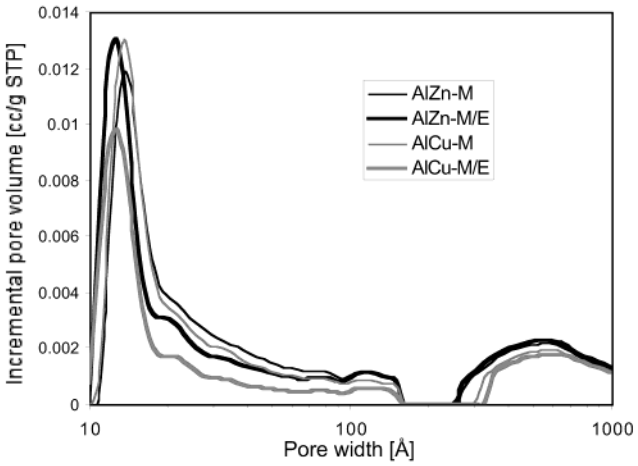

Figure 5. Comparison of pore size distributions for Zn- and Cu-doped samples before and after H_2S adsorption.

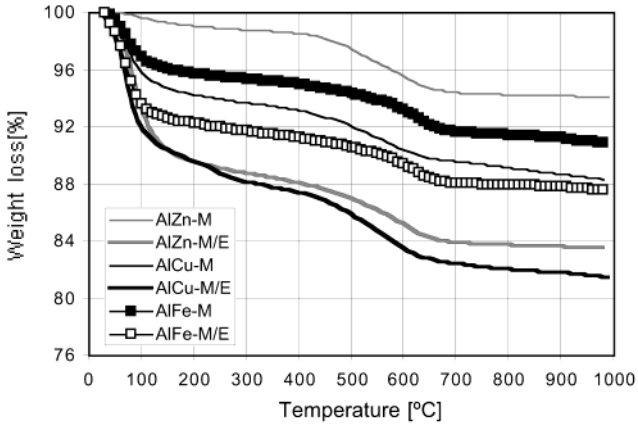

Figure 6. TG curves in nitrogen.

becomes acidic after pillaring because of the dehydration and the dehydroxylation of the Keggin ion at 400 °C and the formation of Al_2O_3 pillars. As a result, H^+ cations are generated:

$$2[AlO_4Al_{12}(OH)_{24}(H_2O)_{12}]^{7+} \rightarrow 13Al_2O_3 + 14H^+ + 29H_2O \quad (1)$$

An unchanged pH value for the iron-modified sample supports our hypothesis about the conversion to weakly adsorbed SO_2. A decrease in the pH for AlCu−M/E is related to the formation of new species. This hypothesis is discussed below.

Results of thermogravimetric analyses are collected in Figures 6 and 7. A comparison of TG curves (Figure 6) once again indicates that in the case of the sample modified with iron only adsorbed water or weakly retained SO_2 can be detected. It is seen as an increase in weight loss at about 100 °C. At higher temperatures, the curves remain almost parallel, with a weight loss at about 600 °C related to the dehydroxylation of hydroxyaluminum layers.[30] For the Cu- and Zn-modified samples, an increase in weight loss is noticed after H_2S adsorption.

On DTG curves (Figure 7), the weight losses in certain temperature ranges are represented as peaks whose surface areas can be directly compared. An analysis of the curves obtained for zinc- and copper-modified samples before and after hydrogen sulfide adsorption clearly shows the thermal desorption of new species present on the surface after the materials were exposed to hydrogen sulfide. Because the first peak with a maximum at about 100 °C represents mainly water, its intensity is not discussed here. An interesting temperature range where changes

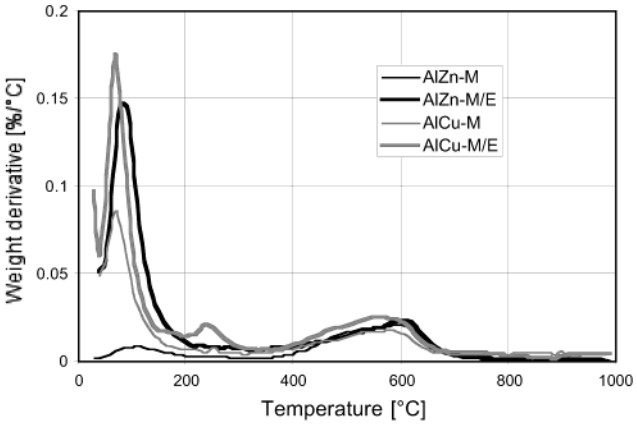

Figure 7. Comparison of DTG curves in nitrogen for Zn- and Cu-doped samples before and after H_2S adsorption.

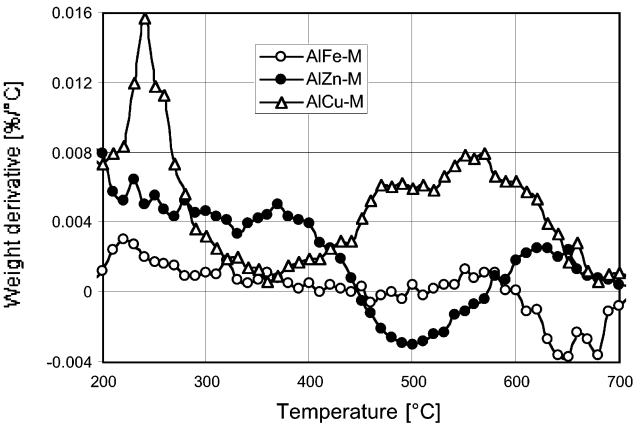

Figure 8. Differences in DTG curves in exhausted and initial samples.

are observed is the one between 200 and 700 °C. To make this more unambiguous, we plotted in Figure 8 the differences between the exhausted and the initial samples. It is clearly seen that whereas for the iron-modified sample the curve is almost flat in the cases of zinc and especially of copper significant features can be noticed. The well-defined peak between 220 and 280 °C likely represents the decomposition of copper sulfide with a boiling point of 220 °C.[48] The second broad peak, between 400 and 700 °C, is the result of the decomposition of copper sulfate (boiling point 650 °C)[48] to sulfur oxide and copper oxide. This latter copper sulfate was likely formed on the surface from copper sulfide when enough oxygen from the air was present for the further oxidation of sulfides. Indeed, for this sample a noticeable decrease in the pH was found after H_2S adsorption.

It is also noteworthy to mention how the samples change their appearance after H_2S adsorption. Although AlFe−M (brick red) and AlZn−M (pale gray) hardly change color after H_2S adsorption (they become slightly lighter), AlCu−M is the only sample that really undergoes a color change, from dark gray to dark green. This supports our hypothesis that first CuS is formed and then it is oxidized to $CuSO_4$ (dark green).

To better understand the mechanisms of H_2S adsorption on the three doped samples, for each sample, the number of moles of doped Me cations, calculated from the percentage of doped Me cations (from elemental analysis), was compared to the number of moles of H_2S adsorbed on the sample, which was evaluated from the breakthrough capacity results. The results are collected in Table 3. It is interesting that for AlZn−M the number of moles of metal and hydrogen sulfide are identical,

TABLE 3: Number of Moles of Metals Doped on the Surface and Number of Moles of Hydrogen Sulfide Adsorbed

sample	Me [mmol/g]	H_2S [mmol/g]
AlFe−M	1.70	0.51
AlZn−M	0.61	0.61
AlCu−M	1.10	1.43

which suggests a direct chemical reaction between zinc and hydrogen sulfide and optimum conditions of doping manifested by the accessibility to all of the zinc cations. In the case of AlCu−M, the number of moles of doped Cu is 30% smaller than the number of moles of adsorbed H_2S. This indicates that on the surface of this material there are copper cations that can act as catalysts for H_2S oxidation. However, for AlFe−M, the number of moles of doped Fe^{3+} cations far exceeds (by a factor of more than 3) the number of moles of H_2S, which suggests that most Fe^{3+} in AlFe−M do not participate in H_2S immobilization. It is likely that the doping level was too high. Excess Fe^{3+} resulted in the destruction of micropores and the formation of large iron clusters. Another reason for this may be the difference in the oxidation states of iron (+3) and copper and zinc (+2).

On the basis of the results described above addressing the chemical structure and performance of materials such as hydrogen sulfide adsorbents, the mechanism for H_2S immobilization on Me-doped Al−M seems to be based on acid−base reactions. In the first step, H_2S is adsorbed on the sample surface through a metathesis reaction, where hydrated Me^{n+} acts as a Lewis acid toward the base S^{2-} and H^+ and H_2O compose the other acid−base pair:

$$Me^{n+}(H_2O)_m + H_2S \rightarrow MeS^{(n-2)+}(H_2O)_{m-2} + 2H_3O^+ \quad (2)$$

Indeed, Lewis acids and bases preferentially bind if they are both hard or soft.[49,50] Although H^+ and H_2O are both considered to be hard species, S^{2-} is a soft base.[51] However, Fe^{3+} is a hard acid, whereas Zn^{2+} and Cu^{2+} are borderline acids (which means that they are halfway between hard and soft acids).[50] Consequently, when the formation of metal sulfide with Zn^{2+} and Cu^{2+} is very favorable, only a weak bond with Fe^{3+} can form. This would explain why chemisorption occurs more favorably on AlZn−M and AlCu−M than on AlFe−M. Without doping, the only available Lewis acids are Si^{4+} and Al^{3+}, which are also strong acids. But because they belong to the clay layers or to the pillars, they are bound to O^{2-}, a hard base,[50] which makes them even harder acids,[49] especially harder than Fe^{3+}. Binding S^{2-} to these cations is then unlikely, which explains the negligible capacity that was found for Al−M. The H_3O^+ formed during this first step would be responsible for the pH decreases observed with AlZn−M and AlCu−M. These sulfides can be oxidized to sulfates by oxygen from the air, and the occurrence of this process was observed in the case of the AlCu−M sample. Taking into account that water is present in the system and adsorbed in pores, $CuSO_4$ dissociates, leaving copper ion available to bind S^{2-} further. This can account for the fact that the amount of H_2S that is adsorbed is greater than the number of copper ions introduced to the surface of the mineral. Because the amount of copper sulfate dissolved is limited by the amount of water adsorbed in pores, the breakthrough occurs when no more H_2S can react on the surface. Moreover, another product of the surface reaction is sulfur dioxide, whose low concentration (a few ppm) was detected in the effluent gas.

The smaller capacity for hydrogen sulfide immobilization observed for the zinc-doped material is due to the smaller doping effect than in the case of copper (twice as much copper as zinc). To explain the "catalytic" effect of copper (more moles of H_2S adsorbed than Cu cations present), the kinetics of sulfide oxidation should be considered. Because in the case of the copper-doped material the number of binding sites for sulfur was greater than in the case of the zinc-doped counterpart, the breakthrough to 1000 ppm of H_2S for the former sample took longer than for the latter one. The consequence of this is the longer contact of CuS with oxygen than that for ZnS. These differences in time would be critical for the oxidation of sulfides to sulfates. In fact, in the case of AlZn−M, changes in the slope of the breakthrough curves could be noticed. This phenomenon can be related to the initialization of ZnS oxidation on the surface. Besides this, there are also differences in the solubility constants for CuS and ZnS. Because K_S for CuS is equal to 1.27×10^{-36} compared to 2.93×10^{-25} [48] for ZnS, the formation of CuS is more favorable than the formation of ZnS.

In the case of AlFe−M, where Fe^{3+} rather than Fe^{2+} ions are present on the surface, the mechanism of H_2S immobilization can differ from that for copper and zinc. This is the result of differences not only in the nature of metal cations (degree of oxidation) but also in their spatial distributions. As indicated above, in the case of iron, only a part of it is exposed to the surface, owing to hydrolysis and the propensity of iron to adsorb on the surface in the form of clusters.[35,36] The iron species, which are exposed, are reduced to Fe^{2+}, causing H_2S to be oxidized to sulfur. H_2S is easily oxidized to sulfur, which is weakly adsorbed on the surface, because of the lack of microporosity. Indeed, the measurement of the SO_2 concentration in the effluent gas revealed the presence of 1 ppm of sulfur dioxide when the breakthrough concentration of H_2S was 350 ppm. (In the case of copper- and zinc-modified clays, the level of sulfur dioxide reached only 0.3 ppm at 350 ppm of hydrogen sulfide in the effluent gas.) SO_2 is easily desorbed when the clay is exposed to ambient conditions. Thus, the products of surface reactions/oxidation are not detected on the surface.

Conclusions

Doping of montmorillonite pillared with aluminum oxides with Fe^{3+}, Zn^{2+}, or Cu^{2+} results in a significant increase in hydrogen sulfide adsorption on the surface. As a result of surface reaction, hydrogen sulfide is immobilized as metal sulfides. Because of the presence of oxygen in the system, further oxidation occurs, and sulfates are formed. The best performing materials are the ones doped with Cu, which is due to the high propensity of copper to form sulfides. When iron was present, the removal of hydrogen sulfide was not efficient because of the clustering of iron and the oxidation of H_2S to elemental sulfur and then to SO_2, which is very weakly adsorbed on the surface.

Acknowledgment. We thank Professor Maria Tamargo and Ms. Yanting Liao for XRD measurements. This work was partially supported by PSC-CUNY (grant no. 64358-00-33).

References and Notes

(1) Brindley, G. W.; Sempels, R. E. *Clay Miner.* **1977**, *12*, 229.
(2) Lahav, N.; Shani, U.; Shabtai, J. *Clays Clay Miner.* **1978**, *26*, 107.
(3) Loeppert, R. H.; Mortland, M. M.; Pinnavai, T. J. *Clays Clay Miner.* **1979**, *27*, 201.
(4) Pinnavaia, T. J. *Science* **1983**, *220*, 356.
(5) Cheng, L. S.; Yang, R. T. *Microporous Mater.* **1997**, *8*, 177.
(6) Hernando, M. J.; Pesquera, C.; Blanco, C.; Gonzalez, F. *Chem. Mater.* **2001**, *13*, 2154.
(7) Hutson, N. D.; Gualdoni, D. J.; Yang, R. T. *Chem. Mater.* **1998**, *10*, 3707.
(8) Gil, A.; Guiu, G.; Grange, P.; Montes, M. *J. Phys. Chem.* **1995**, *99*, 301.
(9) Plee, D.; Borg, F.; Gatineau, L.; Fripiat, J. J. *J. Am. Chem. Soc.* **1985**, *107*, 2362.
(10) Jagiello, J.; Bandosz, T. J.; Schwarz, J. A. *Langmuir* **1997**, *13*, 1010.
(11) Bandosz, T. J.; Jagiello, J.; Schwarz, J. A. *J. Phys. Chem.* **1996**, *100*, 15569.
(12) Zhu, H. Y.; Zhu, Z. H.; Lu, G. Q. *J. Phys. Chem. B* **2000**, *104*, 5674.
(13) Choy, J. H.; Park, J. H.; Yoon, J. B. *J. Phys. Chem. B* **1998**, *102*, 5991.
(14) Bandosz, T. J.; Cheng, K. *J. Colloid Interface Sci.* **1997**, *191*, 456.
(15) Yang, R. T.; Baksh, M. S. A. *AIChE J.* **1991**, *37*, 679.
(16) Martin-Luengo, M. A.; Martins-Carvalho, H.; Ladriere, J.; Grange, P. *Clay Miner.* **1989**, *24*, 495.
(17) Figueras, F.; Martrod-Bashi, A.; Fetter, G.; Therier, A.; Zanchettr, J. V. *J. Catal.* **1986**, *34*, 658.
(18) Choudary, B. M.; Valli, V. I. K. *J. Chem. Soc., Chem. Commun.* **1990**, 1115.
(19) Pinnavaia, T. J.; Landau, S. D.; Tzou, M. S.; Johnson, I. D. *J. Am. Chem. Soc.* **1985**, *107*, 7222.
(20) Galarneau, A.; Barodawalla, A.; Pinnavaia, T. J. *Nature* **1995**, *374*, 529.
(21) Jones, S. L. *Catal. Today* **1987**, *12*, 209.
(22) Yamanaka, S.; Doi, T.; Sako, S.; Hattori, M. *Mater. Res. Bull.* **1984**, *19*, 161.
(23) Occelli, M. L. *J. Mol. Catal.* **1986**, *35*, 377.
(24) Mitchell, I. V. *Pillared Layered Structures: Current Trends and Applications*; Elsevier: London, 1970.
(25) Jamis, J.; Drljaca, A.; Spiccia, L.; Smith, T. D. *Chem. Mater.* **1995**, *7*, 2078.
(26) Thomas, S. M.; Bertrand, J. A.; Occelli, M. L.; Huggins, F.; Gould, S. A. C. *Inorg. Chem.* **1999**, *38*, 2098.
(27) Adib, F.; Bagreev, A.; Bandosz, T. J. *Environ. Sci. Technol.* **2000**, *34*, 686.
(28) Bandosz, T. J. *J. Colloid Interface Sci.* **2002**, *1*, 246.
(29) Bagreev, A.; Bashkova, S.; Locke, D. C.; Bandosz, T. J. *Environ. Sci. Technol.* **2001**, *35*, 1537.
(30) Grim, R. E. *Clay Mineralogy*; McGraw-Hill: New York, 1968.
(31) Ohtsuka, K. *Chem. Mater.* **1997**, *9*, 2039.
(32) Bond, G. C. *Heterogeneous Catalysis*; Clarendon Press: Oxford, U.K., 1974.
(33) Halsey G. J. *J. Chem Phys.* **1948**, *16*, 931.
(34) Androutsopoulos G. P.; Constantinos, E. S. *Ind. Eng. Chem. Res.* **2000**, *39*, 3747.
(35) Bakas, T.; Moukariaka, A.; Papaefthymiou, V.; Ladavos, A. *Clays Clay Miner.* **1994**, *42*, 634.
(36) Chen, J. P.; Hausladen, M. C.; Yang, R. T. *J. Catal.* **1995**, *151*, 135.
(37) Thomas, J. M.; Thomas, W. J. *Principles and Practice of Heterogeneous Catalysis*; VCH: New York, 1996.
(38) Bandosz, T. J.; Jagiello, J. Schwarz, J. A. *J. Phys. Chem.* **1996**, *100*, 15569.
(39) Saito, A.; Foley, H. C. *AIChE J.* **1991**, *37*, 429.
(40) Olivier, J. P.; Occelli, M. L. *J. Phys. Chem. B* **2001**, *105*, 623.
(41) Jagiello J.; Bandosz, T. J.; Schwarz, J. A. *Langmuir* **1997**, *13*, 1010.
(42) Gil, A.; Grange, P. *Langmuir* **1997**, *13*, 4483.
(43) Yang, R. T.; Baksh, M. S. A. *AIChe J.* **1991**, *37*, 679.
(44) Baksh, M. S.; Yang, R. T. *AIChe J.* **1991**, *37*, 923.
(45) Bandosz, T. J. *Pol. J. Chem.* **1998**, *72*, 1202.
(46) Nguyen-Thanh, D.; Bandosz, T. J. *Phys. Chem. Chem. Phys.*, submitted for publication.
(47) Sterling, D. *The Sulfur Problem: Cleaning Up Industrial Feedstocks*; Royal Society of Chemistry: Cambridge, U.K., 2000.
(48) *CRC Handbook of Chemistry and Physics*, 62nd ed.; CRC Press Inc.: Boca Raton, FL, 1981−1982.
(49) Finston, H. L.; Rychtman, A. C. *A New View of Current Acid−Base Theories*; Wiley: New York, 1982.
(50) Ho, T. L. *Hard and Soft Acids and Bases Principle in Organic Chemistry*; Academic Press: New York, 1977.
(51) Shriver, D. F.; Atkins, P. *Inorganic Chemistry*, 3rd.; W. H. Freeman: New York, 1999.